

The relationship between electric processing condition and microstructure in the solidification of multicomponent oxides

Ashutosh Bhagurkar, Rongshan Qin *

School of Engineering & Innovation, The Open University, Walton Hall, Milton Keynes, MK7 6AA, United Kingdom

ARTICLE INFO

Handling Editor: Dr P. Vincenzini

Keywords:

- A. Grain growth
- B. Porosity
- C. Thermal conductivity
- E. Refractories

ABSTRACT

Systematic characterization for the relationship between the electropulse processing conditions and microstructure has been carried out in the present work. It is found that electropulse can refine porosity and alter grain morphology considerably. A processing with optimum electropulsing parameters can reduce over 75% volume fraction of porosity and more than 70% average pore diameter in comparison with that of reference sample without electric treatment. Electric current treatment promotes the growth of dendrites with smaller thickness of primary arms dendrite and prevents the liquid entrapping between the growing solid grains. The former is caused by the effect of electricity-enhanced kinetic mobility on the radius of curvature at the tip of dendrite. The latter is attributed to the effects of electric thermodynamics on the microstructural formation such as the enhanced connectivity of conductive phase. The microstructures obtained by electropulsing treatment are favourable for heat conduction, structural strength and crack prohibition. However, the excess pulse frequency and pulse width can generate unwanted heat to counteract electric effect. The research reveals the relationship between electric processing conditions and microstructure in a perfectly controversial solidification condition in oxide materials to that of the metals and alloys. The results confirm from the opposite side the validity of the pulsed solidification.

1. Introduction

Solidification behaviour of multicomponent oxides is important in many engineering applications and product manufacturing [1]. An example is in continuous casting, where a layer of multicomponent oxides film is built between the copper mould and solid metal shell to play the dual role of controlling horizontal heat extraction and lubrication [2]. Porosity is undesirable in some cases because it reduces heat conduction, causes materials fragmentation and leading to sticking between the casting materials and the mould [3]. Similarly, there are many other cases where porosity reduction in oxide materials is critical [4].

Refinement of porosity in casting has proved to be a non-trivial task. Pores are formed due to two major reasons, namely the density difference between the solid and liquid phases and the gaseous formation/entrapping during the processing. Reduction of porosity can be achieved, in principle, by preventing the trapping of liquid phase within solid grains or dendrites arms so that the volume shrinkage arising from solidification can be compensated by liquid and the gas bubbles can escape via the liquid channel [5]. Large scale casting of metals and alloys

deploys a peculiar temperature distribution to optimize the geometry and velocity of solid-liquid interface to minimize liquid entrapment and pores formation. However, this technique is difficult to implement in case of oxides casting and low dimensional materials solidification. This is due to complex chemistry of multicomponent oxides, higher melting temperature and viscous nature of melt. This work presents electropulsing as a novel technique for controlling porosity in complex oxide materials.

For the oxides considered in the present work, electricity is conducted by the ions instead of electrons. The solid phase has much lower electrical conductivity than that of the liquid [2,6]. This situation is in contrast to the solidification of metals and alloys. The latter has higher electrical conductivity in solid phase than that of the liquid (typically 10% higher at the same temperature and pressure for pure metals). According to the numerical calculation based on Landau theory [7], electric processing promotes the nucleation and growth of the phases with relatively higher electrical conductivity than that in the matrix [8]. Experimental observations have confirmed such effect of electric treatment on the microstructural evolution in the solidification of cast iron

* Corresponding author.

E-mail address: rongshan.qin@open.ac.uk (R. Qin).

<https://doi.org/10.1016/j.ceramint.2023.03.133>

Received 9 January 2023; Received in revised form 24 February 2023; Accepted 13 March 2023

Available online 16 March 2023

0272-8842/© 2023 The Authors. Published by Elsevier Ltd. This is an open access article under the CC BY license (<http://creativecommons.org/licenses/by/4.0/>).

Table 1

The chemical constitution of the multicomponent oxide (wt.%).

CaO	SiO ₂	Na ₂ O	Al ₂ O ₃	F	MnO	Fe ₂ O ₃	MgO	TiO ₂	K ₂ O	Others
33.60	24.00	9.23	9.07	7.92	7.13	1.16	0.95	0.37	0.17	6.4

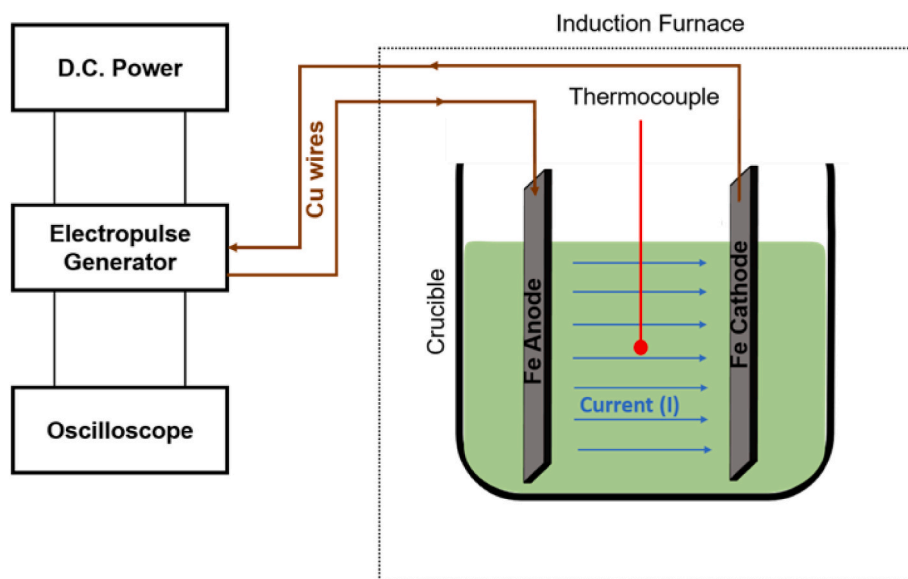


Fig. 1. Schematic diagram for the experimental setup [19] (online color only). (For interpretation of the references to color in this figure legend, the reader is referred to the Web version of this article.)

[9], solders [10] and light alloys [11]. Many large scale industrial casters have adopted this method and achieved significantly higher fraction of equiaxed grains and lower fraction columnar grains [12]. This is because the directional growth of dendrite is disrupted by the electric current promoted nucleation in the molten materials ahead of the solidification front. Thermodynamic calculations suggest that electric processing will suppress the nucleation and growth of solid phase in the solidification of oxide materials where solid phase has less electrical conductivity than that of the liquid. This phenomenon however, has not been studied previously in great detail.

Another significant effect of electrical treatment is on the kinetic mobility. For example, electropulse can increase the solute diffusivity by over 1000 times when the current density is above a critical value [13]. This forms basis of electroplasticity [14], which has seen wide applications in surface treatment [15,16] and deformation of brittle materials [17]. The micro-mechanism behind the electropulse-enhanced mobility has been observed by advanced characterization method recently [18].

The aim of the present work is to systematically characterize the microstructural formation under the influences of electrical treatment with both added mechanisms of electric thermodynamics and electricity-enhanced kinetic mobility. The materials and experimental procedures are described in section 2. The experimental results are presented in section 3. Section 4 is the discussion for the fundamental understanding, followed by the conclusions and remarks in section 5.

2. Experiments

The materials in the present work have a chemical constitution listed in Table 1, where 'others' in the last column represents carbon and bicarbonates. The sample materials are obtained after heat treatment of an as-received mould powder from a project collaborator at Sandvik AB in Sweden. The powder was heated to 1173 K and maintained for 4 h in order to remove H₂O, some carbonaceous and volatile constituents. The resultant sample was placed in a graphite crucible and then molten by

Table 2

Electropulsing processing parameters.

Sample	Peak electric current (A)	Pulse frequency (Hz)	Pulse width (μs)
REF	0	0	0
A	50	100	60
B	50	500	60
C	50	1000	60
D	50	100	100
E	50	500	100
F	50	100	200
G	100	100	100
H	100	500	100
J	160	1000	60
K	160	100	100
L	160	100	500

induction heating in an open environment. The cylindrical crucible has an inner diameter of 45 mm and a height of 80 mm. The powders were about 80% full at beginning. The crucible was fully embedded in a hole of the induction heating zone. The induction furnace has a power to melt 1 kg stainless steel within 15 min. Solidification experiments were conducted only after the induction heating was turned off. This procedure is important for safety reason because the induced current has the potential to damage the electric processing facilities even if they are switched off.

The electric treatment facilities are demonstrated schematically in Fig. 1 [19]. A DC power (Delta Electronika, SM1500 series) converts the alternating current from 230 V to direct current at 24 V. The maximum output power for the device is 80 W only. The pulse generator (AVTECH, AV-108F-2-B-P) converts the direct current to square-wave electric current pulses with adjustable parameters in a range of: peak current from 0 to 200 A, pulse duration from 20 μs to 1 ms and pulse frequency from 1 Hz to 1000 Hz. An oscilloscope is used to monitor the electropulse signal. The electric current pulses are output through two copper cables and linked to anode and cathode respectively. The electrodes are

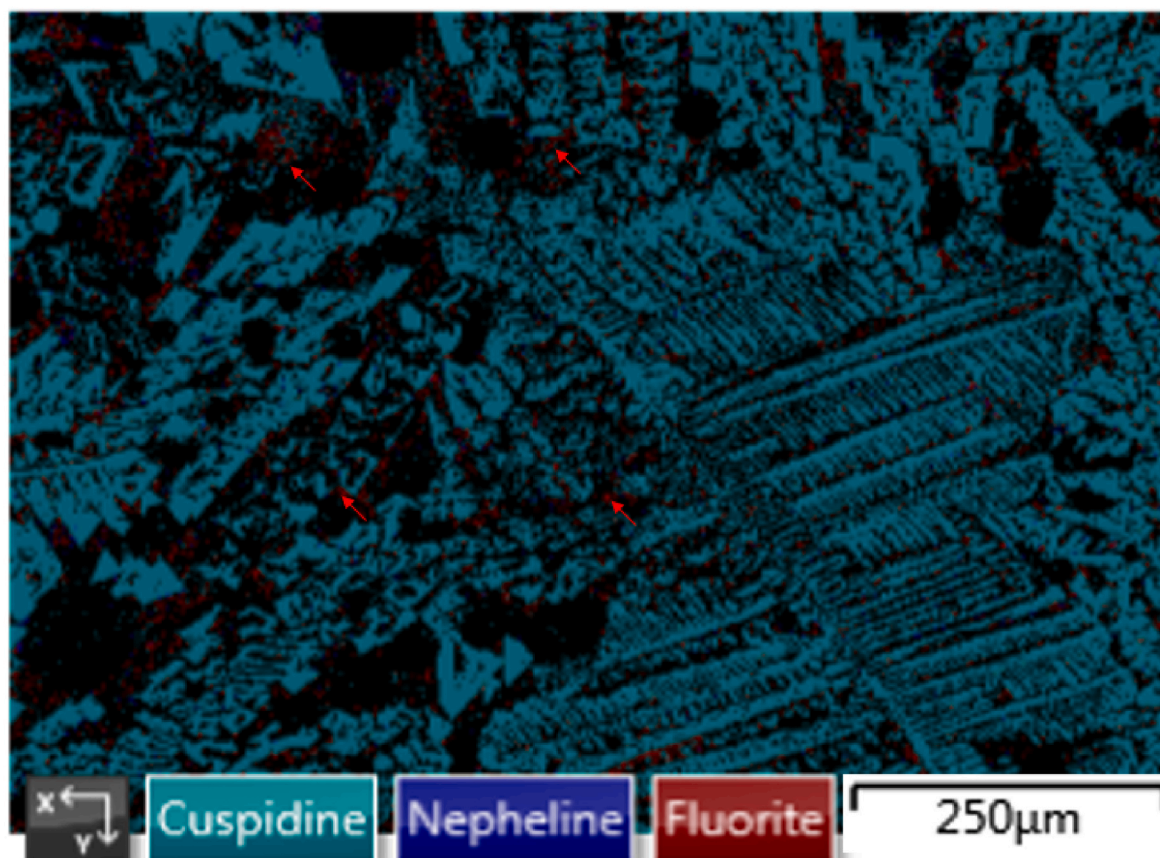


Fig. 2. EMSD image for the Ref sample demonstrates the solidification sequences. The primary dendritic grains are cuspidine crystals. Some of the finally solidified fluorite crystals are denoted by the red arrows (online color only). (For interpretation of the references to color in this figure legend, the reader is referred to the Web version of this article.)

pure iron rods with rectangular cross-section of 8 mm × 6 mm. After turning off the induction heating, both preheated electrodes are inserted to the molten oxide materials from top to almost the bottom of the molten oxides. The distance between the electrodes is about 12 mm from edge to edge. All the samples have electrodes inserted in the liquid before solidification. This is to ensure identical thermal (temperature distribution) and mechanical (disturbance of liquid due to inserting of electrode) conditions for all the samples without and with various electric treatments. The only differences in the processing conditions are from electric parameters, which are listed in Table 2.

Electric treatment last for 30 min for each sample. This ensures the samples to solidify completely. Electrodes are then pulled out of the samples easily due to non-wettability between iron and oxides. The samples were cut along the longitudinal section, polished and examined by optical microscope and scanning electron microscopy (Zeiss Supra 55VP FEG SEM). The microstructures demonstrated in the present work are from the central places between the two electrodes. These places have the highest electric current density and are least affected by the temperature and mechanical disturbances caused by the inserting of electrodes.

For the experimental setup implemented in the present work, the electric current density is distributed heterogeneously. This is because the electrical resistances at different electric current flow paths are different due to the variant lengths of the paths. A longer path has lower current density due to higher electrical resistance between two constant electrical potential electrodes. In contrast, the shortest path between the electrodes has the least resistance and thus the highest current density. As a result, the effect of electric treatment on the microstructure is most pronounced in the region between the electrodes. However, it is possible to design the current density to be more homogeneous in practical using

different geometry and configurations of electrodes and melting devices.

The images obtained from the microscopes were analysed using Image J software in order to find out the effect of electric treatment on the evolution of porosity in the solidified samples.

3. Results

The solidification follows a phase formation sequence of cuspidine ($2\text{SiO}_2 \cdot 3\text{CaO} \cdot \text{CaF}_2$), nepheline ($\text{NaAlSi}_2\text{O}_6$) and fluorite (CaF_2) [20]. The solidification sequence can be seen clearly from an Electron Backscatter Diffraction (EBSD) phase map shown in Fig. 2. According to thermodynamic calculation and measurement of electric current [20], cuspidine forms the primary dendritic grains at 1423 K. cuspidine and nepheline form eutectic structure from the residual liquid when the temperature is lower than 1193 K. Ionic fluorine has high electrical conductivity in liquid state but solidifies to form CaF_2 at 890K. All the phases have much lower electrical conductivity in solid than that in the liquid states. According to the experimental measurement (shown in Fig. 6 at Ref. 20), the highest temperature at the central position is cooled down to 540 K after 30 min of electric treatment. The solidification in the samples has completed before this time.

Experiments have been carried out for many times for each set of parameters. Many images have been obtained via surface characterization. The images presented in the present work are generally representative rather than selective. Fig. 3 presents the SEM images for (a) the reference sample (REF) without electrical field applied to it during solidification; (b) the sample A treated by electropulse with pulse width of 60 μs, (c) the sample D treated by electropulse with pulse width of 100 μs, and (d) the sample F treated by electropulse with pulse width of 200 μs. In all the three electric treated samples the peak electric current was 50

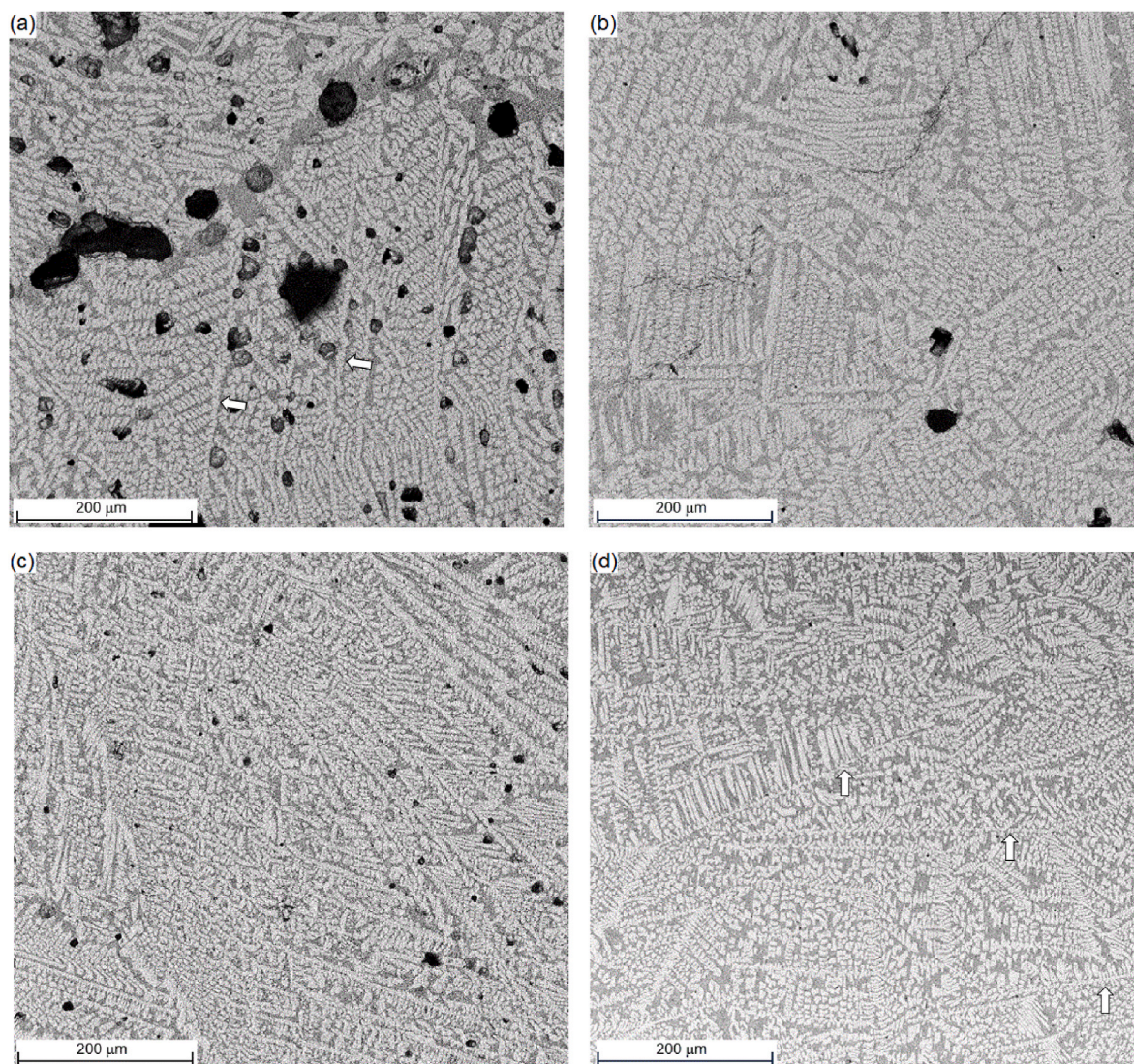


Fig. 3. The SEM images for samples (a) REF, (b) A, (c) D and (d) F. The black areas represent the pores. The white arrows in (a) and (d)m indicate the possible primary dendritic arms.

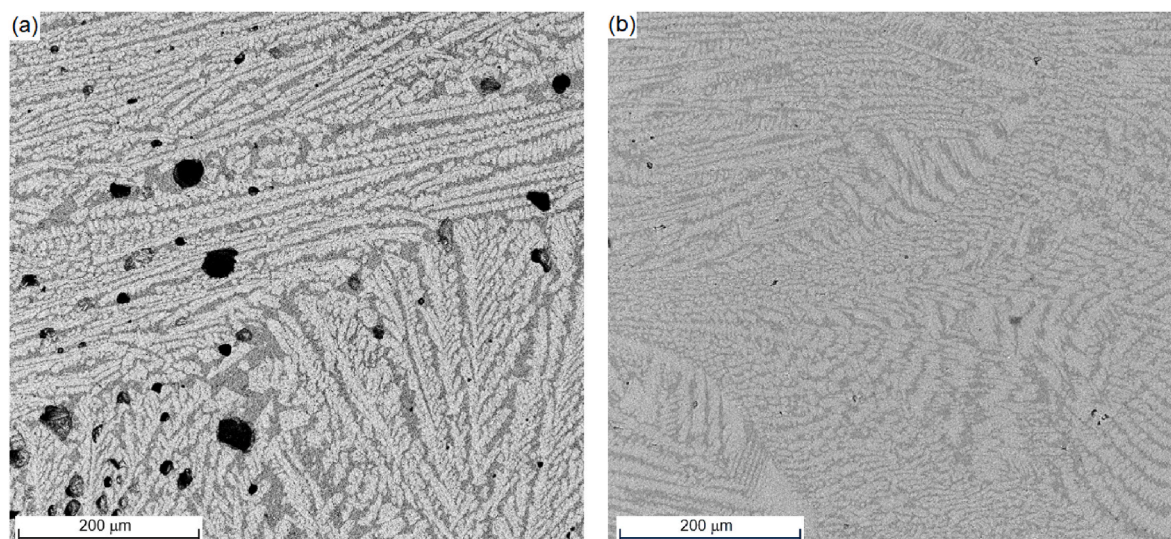


Fig. 4. The SEM images for samples (a) E and (b) H. Both have same pulse width of 100 μ .

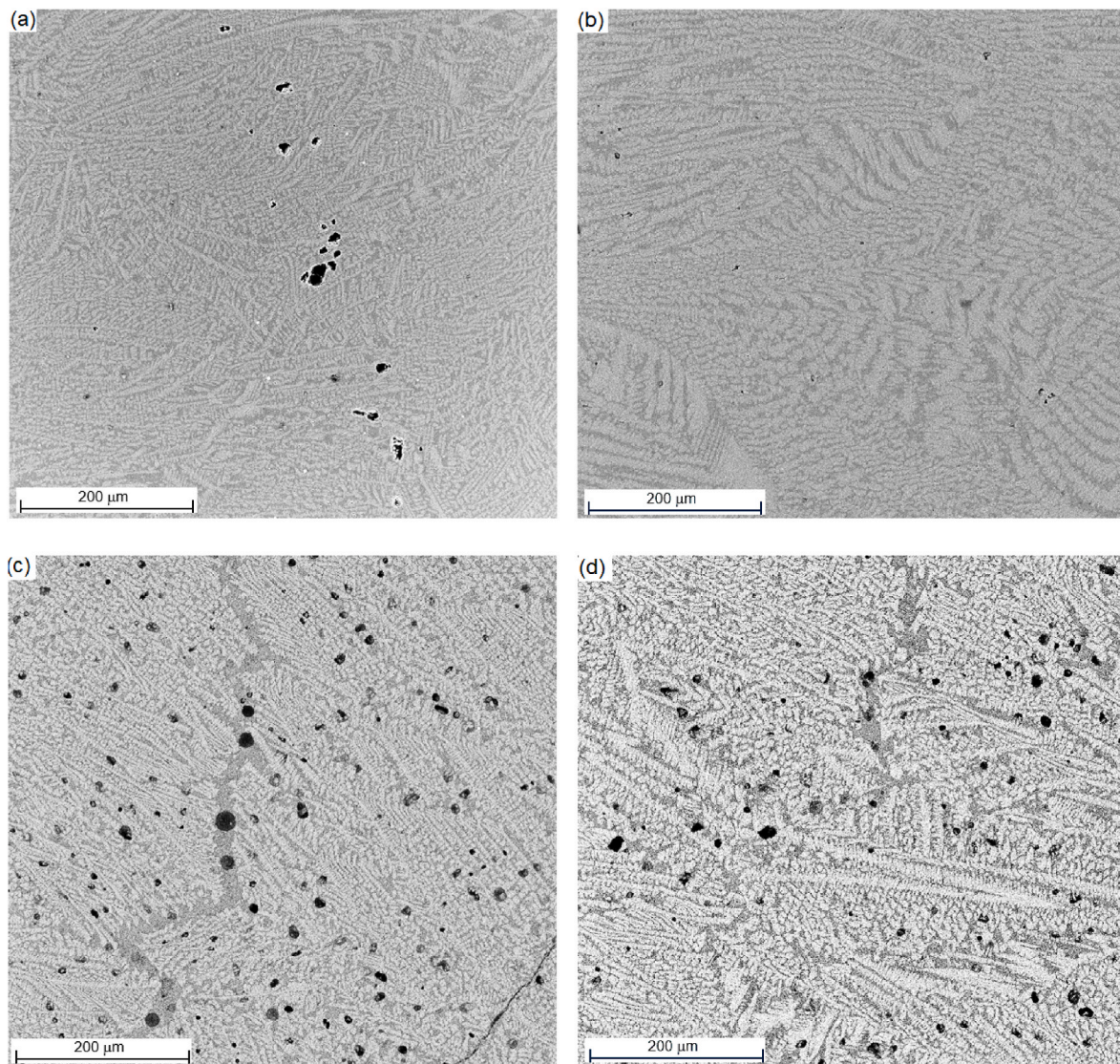


Fig. 5. The SEM images for samples (a) G, (b) H, (c) B and (d) C. (a) and (b) were treated by the same electric pulse width of 100 μ s. Fig. 5(d) is same to Fig. 4(b). They are put together for the convenience of comparison.

A and the pulse frequency was 100 Hz. It can be seen that the porosity has changed significantly by electric processing. Fig. 3(a) has significant amount porosity and the size of some of the pores is relatively large. However, Fig. 3(d) only shows some tiny pores. In the given peak current and pulse frequency, 200 μ s pulse width results in effective porosity minimization than that of 100 μ s and 60 μ s electrical parameters.

Fig. 4 shows the microstructure change when the peak electric current changes from (a) 50 A to (b) 100 A, while the pulse width and frequency remains the constant (100 μ s and 500 Hz, respectively). It can be seen clearly that the number of large pores decrease when the peak current increases. The microstructures are quite different when the peak current changes. More densely distributed interconnective liquid channels are observed in Fig. 4(b) in comparison with that in Fig. 4(a).

In order to study the effect of pulse frequency on the microstructural evolution, two sets of images are shown in Fig. 5 for comparison. The samples in Fig. 5(a) and (b) (identical to Fig. 4(b)) have been electric processed using the same pulse width of 100 μ s and the same peak current 100 A. However, the pulse frequency has been changed from 100 Hz in Fig. 5(a) to 500 Hz in Fig. 5(b). Microstructural coarsening has been observed in high frequency electric current processing while porosity is low. Fig. 5(c) and (d) show the microstructures after electric treatment of 60 μ s pulse width and 50 A peak current and frequency of

500 Hz in Figs. 5(c) and 1000 Hz in Fig. 5(d). It can be seen that cuspidine dendrites have coarsened in comparison with Fig. 5(a and b) with no notable porosity reduction. This suggests that when the peak current is also high, the high frequency treatment can counteract desired microstructure modifications. An example is the sample J, where both large pore and coarsen microstructures are observed, as is shown in Fig. 6. Therefore, the frequency above 500 Hz is not recommended for electric processing.

Similarly, It is also not to recommend to use excess long pulse width. Fig. 7 demonstrates the microstructures from sample K and L. Both samples were electric treated with 160A peak current and 100 Hz frequency but Fig. 7(a) is the sample treated by pulse width 100 μ s and Fig. 7(b) by 500 μ s. It can be seen that the dendritic arms are much coarser in Fig. 7(b) than Fig. 7(a). Combined analysis of Figs. 3 and 7 suggests that it is recommended to optimize the value for the pulse width in order to obtain desirable microstructure.

4. Discussion

Electric processing imposes two effects, namely the Ohm heating and electric effect itself. Ohm heating causes the temperature rising in the sample, which can be calculated using the following equation [21].

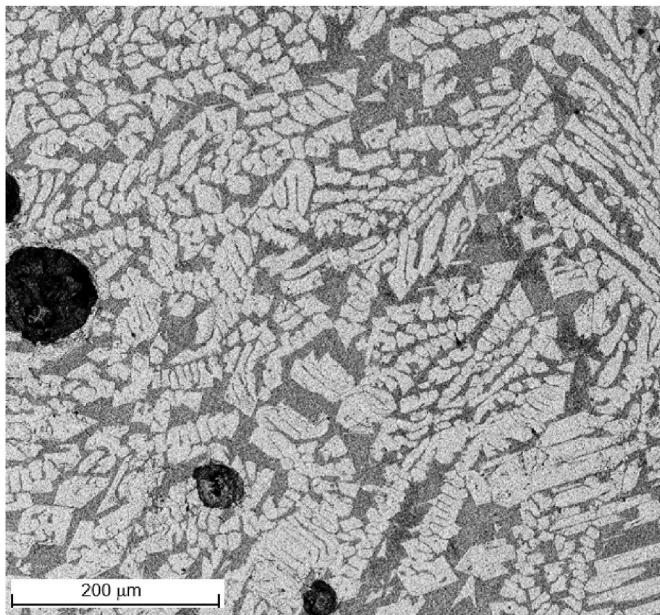


Fig. 6. The SEM image for sample J shows large pore and coarse grains.

$$\Delta T = \frac{\rho_e I^2 f \Delta t_d}{c \rho_d s_{eff}^2} \quad (1)$$

where ρ is the electrical resistivity, c the specific heat, ρ_d the density, s_{eff} the effective cross section area. Those parameters are either materials properties or dimensions of sample that are not relevant to the electric processing conditions. The electric processing conditions are I , f and Δt_d standing for electric current, pulse frequency and pulse width. For the samples considered in the present work, $I^2 f \Delta t_d$ has the values listed in Table 3. Those values were calculated according to the parameters (I , f and Δt_d) listed in Table 2. The effect of Ohm heating on sample J is very high. The next highest one is for sample L. This explains the detrimental effect observed in sample J and significant grain coarsening observed in sample L, as are shown in Figs. 6 and 7(b). In the experiments, several other samples show significant microstructure deterioration by the excess Ohm heating.

The electric effect itself includes two aspects. Thermodynamically, electric current exerts additional free energy to the phase transition. This is described by the Landau theory [7].

$$E^e = -\frac{1}{2} \int (\vec{H} \cdot \vec{B}) dv \quad (2)$$

where \vec{H} is the magnetic field strength and \vec{B} is the magnetic field. The integration goes throughout the whole space including both inside and outside of the sample materials. Eq. (2) can be represented to another format for the current-induced free energy difference during solidification [8]

$$\Delta E^e = \frac{1}{8\pi} \iint \frac{\mu(v') [\vec{j}_a(v') \cdot \vec{j}_a(v) - \vec{j}_b(v') \cdot \vec{j}_b(v)]}{|v - v'|} dv dv' \quad (3)$$

where $\vec{j}_b(v)$ and $\vec{j}_a(v)$ are the electric current density at a space position within an infinitesimal volume v in the materials before and after the phase transition, respectively. μ is the magnetic permeability. In fact, Eq. (2) can be derived from the work carried out by electric field to the drifting electrons, and Eq. (3) is an alternative expression of Eq. (2) for the convenience of numerical calculation of electric free energy. The details derivation of Eqs. (2) and (3) and the discrete format of Eq. (3) have been published by Qin and Bhowmik [8]. The numerical results for the electric current distribution, electric free energy and Ohm heating-induced temperature rising for the materials studied in the present work in one set of processing parameters have been presented in a separated paper [19]

Numerical calculations for many cases have shown that electric processing promotes the formation of higher conductive state and demote the microstructural evolution toward a system with lower electrical conductive configuration [22,23]. For the oxide materials investigated in the present work, liquid state has significant higher electrical conductivity than that of the solid state [2,6,24]. If some liquids are trapped inside solid phases, that portion of liquid will not be able to contribute to the electrical conductive because it is surrounded by nearly insulated solid phase. For this reason, electric treatment holds a mechanism to prevent the dendrites from growing into a morphology to entrap liquid. Liquid connectivity is improved by the electric processing. The interconnected liquid channel enables the volume shrinkage, during primary dendrite growth, to be filled by oxide melt.

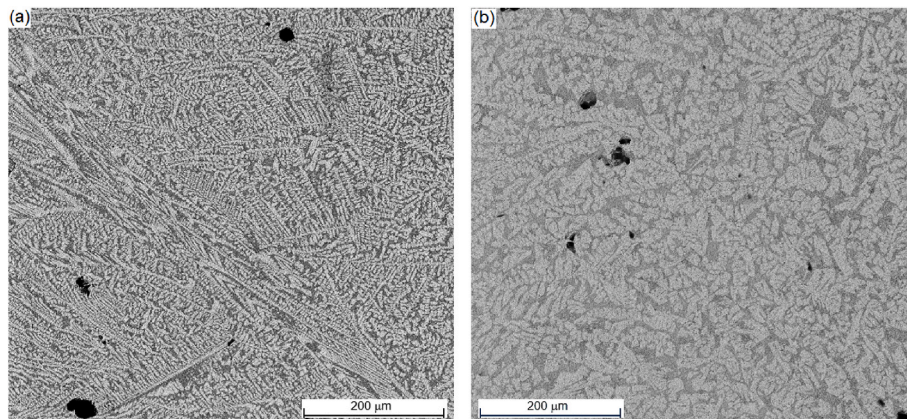


Fig. 7. The SEM images for (a) sample K and (b) sample L.

Table 3

The effect of electric processing conditions on Ohm heating.

Sample	A	B	C	D	E	F	G	H	J	K	L
$I^2 f \Delta t_d$ (A ² ·s)	15	75	150	25	125	50	100	500	1532	256	1280

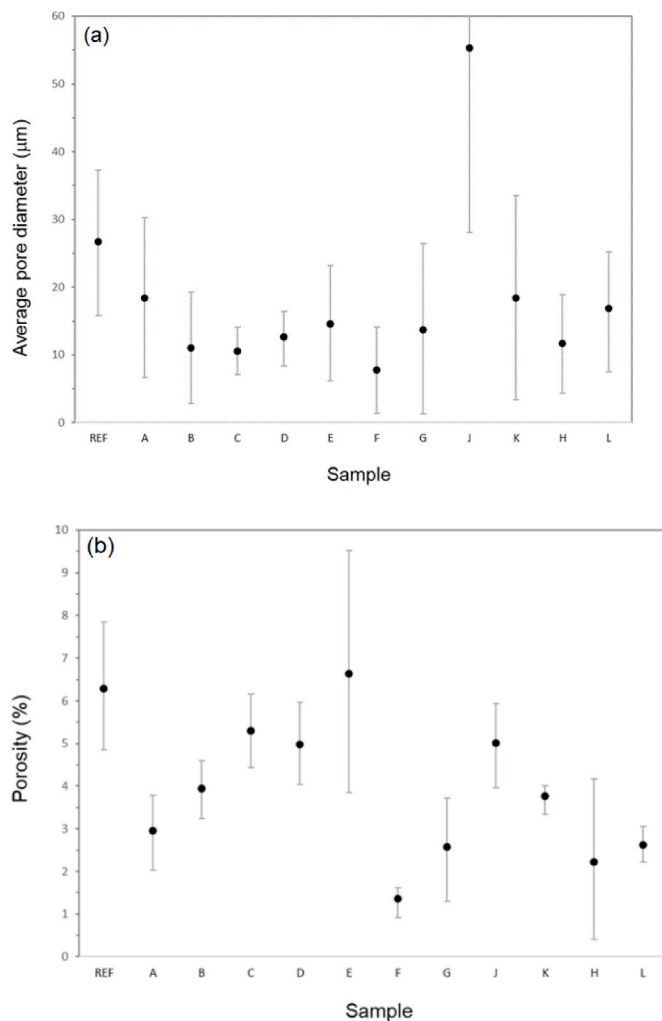


Fig. 8. Numerical calculation results using Image J for (a) the average pore diameter of the samples and (b) the porosity of samples.

On the other hand, the gas bubbles formed during solidification can be escaped via the interconnected liquid channel by means of buoyancy and capillary forces. This is the reason why porosity can be minimized.

From kinetic point of view, electric current enhances mobility over a thousand time [13]. The dendrite tip growth rate in diffusion-controlled crystal growth is proportional to the diffusivity as [25].

$$\vec{v} = -D\nabla u \quad (4)$$

where \vec{v} is the growth velocity, D is diffusivity of solute and ∇u is the gradient of solute composition. When other solidification conditions such as the constitutional undercooling are kept constant, the instability theory shows following growth velocity-radius relation-

$$vR^n = \text{const} \quad (5)$$

where R is the radius of curvature at the tip of dendrite. $n = 1$ for most of the solidification cases [25,26] and $n = 2$ for some other cases [27]. In principle, R can be easily measured according to the thickness of primary arm of a dendrite. However, it is not easy to catch a primary dendritic arm in two-dimensional characterization, especially when the system is not in well-controlled directional solidification. In Fig. 3(a) and (d), some arrows have been added to indicate the possible primary dendritic arms. The thickness in Fig. 3(a) is around 8 μm but that in Fig. 3(d) is less than 3 μm. However, it is worth to point out that the indicated primary dendritic arms might not be in the central part and

hence the estimation is very rough. Eq. (5) shows that the dendritic tip has much smaller radius in the electric treatment than that of the reference samples. This enables formation and growth of thinner dendritic arms, as is observed in all the electric processed microstructures except those coarsening grains caused by excess Ohm heating. The enhanced mobility is also favourable for liquid fluidity and defects annihilation.

According to the energy dispersive spectroscopy (EDS) map reported in our previous work [20], the growth of cuspidine primary dendrite involves the absorption of Ca, Si and F elements and expulsion of Na, Al, Mn and O elements. The diffusion, therefore, involves Ca, Si and F from the liquid oxides toward the solid-liquid interface and Na, Al, Mn and O from the interface to liquid. The diffusivity in Eq. (4) should be the species with slowest mobility. Due to the interactions between metallic and non-metallic elements, the actual diffusivity is likely to be that of an oxide or fluoride. If the gradient of solute composition was known, combination of Eqs. (4) and (5) could be used to determine the effect of electropulsing on the change of diffusivity.

According to Eq. (3), the electric effect is proportional to the current density square. Higher electric current can generate stronger electric effect, which is evident in Fig. 4. However, the electric effect exists only when the electric current passing through the sample. Therefore, more time with electric current should have longer time with electric effect. This explains the observations demonstrated in Fig. 3. But the excess electric current passing time is also accompanied with higher Ohm heating effect. An optimized pulse width and pulse frequency are therefore required to maximize electric effect but minimize Ohm heating effect. This explains the trend shown in Figs. 5–7.

All the SEM images have been analysed using Image J software. Fig. 8 plots the average pore diameter and porosity. The error bars denote the uncertainty in numerical calculation and value fluctuation. Apart from samples J in Fig. 8(a) and E in Fig. 8(b) where excess Ohm heating causes detrimental effects, other samples exhibit less porosity and smaller average pore diameter than that of reference sample. Sample F shows the lowest porosity and smallest average pore diameter. Its porosity is about 21.7% of that in reference sample and its average pore diameter is 29.1% of that in reference sample. This corresponds to >75% reduction of volume fraction of porosity and >70% reduction of average pore diameter in comparison with that in reference samples without electric treatment.

The microstructures in the solidification of oxides are affected by both the electric thermodynamics and electric-enhanced mobility. The thermodynamic effect controls the trends of microstructural evolution such as to promote a phase configuration with higher electrical conductivity. The electric-enhanced mobility accelerates the phase development to achieve the state. Both effects play important roles.

5. Conclusions

Based on experimental characterization and fundamental understanding, the relationship between the electric processing conditions and microstructure have been developed. Following conclusions can be drawn from this investigation.

- Electric processing can significantly affect the microstructure evolution in the solidification of oxides. This includes the morphology of primary dendrite grains, liquid phase connectivity and porosity. Electric processing promotes the formation of thin dendritic arm, interconnected liquid channel and minimized porosity.
- The electric treatment causes two types of effects, namely the Ohm heating and electric effect itself. Ohm heating is determined by the current amplitude, pulse width and pulse frequency. Electric effect is proportional to the electric current density square. Excess Ohm heat can counteract the electric effect.
- Adequate electric processing parameters can reduce >75% volume fraction of porosity and reduce >70% average pore diameter in

comparison with that in reference samples without electric treatment.

- Electric treatment minimises the liquid entrapment between solidified grains and dendritic arm. Furthermore, it also enables the pores formed due to volume shrinkage during solidification to be promptly refilled by the liquid and the gas bubbles to release through the interconnected liquid channels.

Institutional review board statement

Not applicable.

Informed consent statement

Not applicable.

Declaration of competing interest

The authors declare that they have no known competing financial interests or personal relationships that could have appeared to influence the work reported in this paper.

Acknowledgement

The authors are grateful to Karin Hansson-Antonsson and Peter Andersson in Sandvik AB company for provision of oxide powders for making the samples. The research leading to these results received funding from European Commission's Research Fund for Coal and Steel under Grant Agreement No 847269 and from the Engineering and Physical Sciences Research Council at UK under Grant Agreement No EP/X035875/1.

References

- [1] W.L. Wang, X. Yan, L.J. Zhou, H. F. Wu, Q. Zheng, R. Zhao, Influence of electropulsing treatment on crystallization and structure of calcium silicate-based melt, *Ceram. Int.* 49 (2023) 4686–4694.
- [2] K.C. Mills, Structure and properties of slags used in the continuous casting of steel: Part 1 conventional mould powders, *ISIJ Int.* 56 (2016) 1–13.
- [3] M. Massoudi, J. Kim, P. Wang, On the heat flux vector and thermal conductivity of slags: a brief review, *Energies* 9 (2016) 27.
- [4] N.R. Philips, M. Carl, N.J. Cunningham, New opportunities in refractory alloys, *Metall. Mater. Trans. A* 51 (2020) 3299–3310.
- [5] L. Luo, L.S. Luo, Y.Q. Su, L. Su, L. Wang, R.R. Chen, J.J. Guo, H.Z. Fu, Reducing porosity and optimizing performance for Al-Cu-based alloys with large solidification intervals by coupling travelling magnetic fields with sequential solidification, *J. Mater. Sci. Technol.* 79 (2021) 1–14.
- [6] G.H. Zhang, K.C. Chou, Simple method for estimating the electrical conductivity of oxide melts with optical basicity, *Metall. Mater. Trans.* 41B (2010) 131–136.
- [7] W. Eerenstein, N.D. Mathur, J.F. Scott, Multiferroic and magnetoelectric materials, *Nature* 442 (2006) 759–765.
- [8] R.S. Qin, A. Bhowmik, Computational thermodynamics in electric current metallurgy, *Mater. Sci. Technol.* 31 (2015) 1560–1563.
- [9] A.K. Misra, Misra technique applied to solidification of cast-iron, *Metall. Trans. A* 17 (1985) 358–360.
- [10] J.P. Barnak, A.F. Sprecher, H. Conrad, Colony (grain) size reduction in eutectic Pb–Sn castings by electropulsing, *Scripta Metall. Mater.* 32 (1995) 879–884.
- [11] X.L. Liao, Q.J. Zhai, J. Luo, W.J. Chen, Y.Y. Gong, Refining mechanism of the electric current pulse on the solidification structure of pure aluminum, *Acta Mater.* 55 (2007) 3103–3109.
- [12] Q.G. Xue, J.S. Wang, Y.M. He, W.M. Chen, B. Zhu, W.Q. Zhou, Effect of electric pulse inoculation to turkish metal on structure of electrical sheet steel concasting billet, *Spec. Steel* 25 (2004) 53–55.
- [13] H. Conrad, Influence of an electric or magnetic field on the liquid–solid transformation in materials and on the microstructure of the solid, *Mater. Sci. Eng., A* A287 (2000) 205–212.
- [14] M.J. Kim, S. Yoon, S. Park, H.J. Jeong, J.W. Park, K. Kim, J. Jo, T. Heo, S.T. Hong, S. H. Cho, Y.K. Kwon, I.S. Choi, M. Kim, H.N. Han, Elucidating the origin of electroplasticity in metallic materials, *Appl. Mater. Today* 21 (2020), 100874.
- [15] Y.D. Ye, S.Z. Kure-Chu, Z.Y. Sun, X.P. Li, H.B. Wang, G.Y. Tang, Nanocrystallization and enhanced surface mechanical properties of commercial pure titanium by electropulsing-assisted ultrasonic surface rolling, *Mater. Des.* 149 (2018) 214–227.
- [16] S. Akram, A. Babutskyi, A. Chrysanthou, D. Montalvo, M.J. Whiting, N. Pizurova, Improvement of the wear resistance of nickel-aluminium bronze and 2014-T6 aluminium alloy by application of alternating magnetic field treatment, *Wear* 480 (2021), 203940.
- [17] O.A. Troitskii, Electromechanical effect in metals, *JETP Lett.* 10 (1969) 11–14.
- [18] S.T. Zhao, R.P. Zhang, Y. Chong, X.Q. Li, A. Abu-Odeh, E. Rothchild, D.C. Chrzan, M. Asta, J.W. Morris Jr., A.M. Minor, Defect reconfiguration in a Ti–Al alloy via electroplasticity, *Nat. Mater.* 20 (2021) 468–472.
- [19] R.S. Qin, A. Bhagurkar, Effect of pulsating solidification on the surface properties of conductive materials, *Proc. Roy. Soc. A* 478 (2022), 20210726.
- [20] A. Bhagurkar, R.S. Qin, Effect of electropulsing on the solidification of mould flux, *J. Mater. Res. Technol.* 19 (2022) 2146–2155.
- [21] R.S. Qin, A. Rahnama, W.J. Lu, X.F. Zhang, B. Elliott-Bowman, Electropulsed steels, *Mater. Sci. Technol.* 30 (2014) 1040–1044.
- [22] X.F. Zhang, R.S. Qin, Electric current-driven migration of electrically neutral particles in liquids, *Appl. Phys. Lett.* 104 (2014), 114106.
- [23] Y. Zhao, B. He, S. Salliet, C. Domain, P.L. Delliou, M. Perez, R. Qin, Anti-aging treatment of nuclear power plant steel, *Mater. Sci. Eng., A* 735 (2018) 73–80.
- [24] R.S. Qin, Artificial neural network study of the electrical conductivity of mould flux, *Mater. Sci. Technol.* 37 (2021) 1476–1482.
- [25] J.S. Langer, Instabilities and pattern formation in crystal growth, *Rev. Mod. Phys.* 52 (1980) 1–28.
- [26] B.J. Spencer, H.E. Huppert, The relationship between dendrite tip characteristics and dendrite spacings in alloy directional solidification, *J. Cryst. Growth* 200 (1999) 287–296.
- [27] M.B. Koss, J.C. LaCombe, L.A. Tennenhouse, M.E. Glicksman, E.A. Winsa, Dendritic growth tip velocities and radii of curvature in microgravity, *Metall. Mater. Trans. A* 30 (1999) 3177–3190.